Chain Dynamics of Poly(methyl methacrylate) in Dilute Solutions Studied by the Fluorescence Depolarization Method

Takashi Sasaki, Masahide Yamamoto,* and Yasunori Nishijima

Department of Polymer Chemistry, Kyoto University, Kyoto 606, Japan.
Received May 27, 1987

ABSTRACT: Samples of poly(methyl methacrylate) (PMMA) labeled with anthracene in the middle of the chain were synthesized, and their local motions in dilute solutions were examined by the fluorescence depolarization technique. Theoretical functions based on various models for local motions were fitted to the data. The average anisotropy ratio became almost independent of the molecular weight above 1.28×10^5. At high viscosities or at low temperatures, the discrete conformation jump models such as the Jones–Stockmayer (JS) model and the generalized diffusion and loss (GDL) model were in good agreement with the experimental data compared with the models of diffusion on a continuous body such as the Bendler–Yaris (BY) model and the Skolnick–Yaris (SY) model. Plots of dynamic parameters of the Hall–Helfand (HH) model versus viscosity revealed nondiffusive small-scale motions in the higher viscosity region. These findings suggest that some discrete motional modes should be taken into account in order to interpret such small-scale motions. The chain stiffness was evaluated by means of the dynamic parameters of the HH model, and the PMMA chain was found to be relatively rigid compared with the polystyrene chain.

I. Introduction

Investigation of the dynamic properties of polymers is important to understanding the macroscopic behavior of polymer materials. A long flexible polymer chain in dilute solution undergoes a number of internal modes of Brownian motion, and among them, the elementary motions involving conformational transitions usually take place in times on the order of nanoseconds. Investigations of so-called local motions have been done mainly in the following three ways: (1) an idealized model for the local molecular motion is assumed and the experimental observables such as the orientation time-correlation function and the spectral density function are calculated mathematically; (2) the time-correlation function or its spectral density is measured by various experimental tools such as fluorescence depolarization, NMR, and dielectric relaxation, and then the theoretical models are checked, and (3) on the basis of some idealized models, Brownian dynamics simulations are carried out on a computer. Several theoretical models for local motions have been developed during the past 20 years. Since it is almost impossible to treat analytically a model which is faithful to the real chemical structure of a polymer chain, e.g., the rotational isomeric state (RIS) model,[1] the problem is to establish what approximation is appropriate for the real local motions. At the present stage, it seems to be necessary to examine how well the theoretical models explain the experimental data and to reveal the essential feature of local motions. However, the experimental data in this field are insufficient. Experimental studies on various kinds of polymers are also required to solve another interesting problem, the relationship between the local relaxation and the chemical structure of the polymer chain.

Fluoresence depolarization[2] is a powerful tool to investigate local chain dynamics. Anufrieva and her co-workers investigated the dynamics of poly(alkyl methacrylates) by the steady-state measurement of fluorescence depolarization.[3] A recent development of this technique, especially the time-resolved measurements by the single-photon counting method[4] in the nanosecond time region, enables us to observe directly the orientation autocorrelation function of the second moment of the transition vector and to examine closely the agreement between experimental results and theoretical predictions. Valeur and Monnerie[5] investigated the motions of anthracene-labeled polystyrene in dilute solutions by this method to test their tetrahedral lattice model.[6] Recently, Viovy et al.[7] reinvestigated the anthracene-labeled polystyrene system and tested various theoretical models for local motions. Chain dynamics in concentrated solutions[8] and in polymer melts[9] containing a labeled polymer have also been examined by fluorescence depolarization. In addition, torsional and bending motions of nucleic acids have been studied[10] in association with some theories.[11]

We have been studying local chain dynamics by the fluorescence depolarization method and have provided a preliminary report on the anthracene-labeled poly(methyl methacrylate) (PMMA).[12] In the present paper, we report results on higher molecular weight samples of the labeled PMMA and discuss the effect of molecular weight, temperature, and solvent viscosity on the local motions in dilute solutions on the basis of theoretical models. The structure of the polymer used in this study is

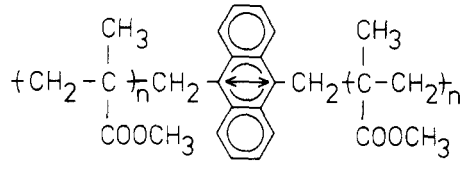

Anthracence is a suitable probe for our study owing to its relatively small size and symmetric shape. Its transition moment, indicated by the arrow, is attached in the middle of the PMMA chain and is parallel to the backbone of the chain. Such a structure seems to be advantageous in discussing various theoretical models of local chain dynamics.

II. Theoretical Background of Local Chain Dynamics

In general, Brownian motions of polymer chains can be treated by the Kirkwood diffusion equation.[13] However, it is difficult to solve this equation under proper conditions based on the details of the real polymer chain. Attempts have therefore been made to formulate certain idealized models for the local structures of polymer chains instead of solving the many-body problem. If the backbone of the polymer consists of a sequence of covalently bonded carbon atoms connected with a fixed angle, there exists a localized kinetic unit involving five bonds (Schatzki crankshaft[14]), and further, if the pentane effect is negligible, a seven-bond kinetic unit exists. If distortion of the bond angle in the course of rearrangement is allowed, kinetic units of 3 and 4 bonds also exist. Mashimo et al.[15] showed by the di-

0024-9297/88/2221-0610$01.50/0

electric relaxation study that crankshaftlike motions are not dominant in a real polymer chain. Liao and Morawetz[16] showed the same result by their intramolecular excimer formation experiments.

Valeur et al.[6] treated theoretically the three-bond jump (Boyer crankshaft) on the tetrahedral lattice (VJGM model). Their master equation (one-dimensional diffusion equation) is

$$\frac{\partial p}{\partial t} = D\frac{\partial^2 p}{\partial x^2} \tag{1}$$

where p is the orientational probability, t the time, x the distance along the chain, and D the diffusion coefficient. By solving this equation, they obtained the orientation autocorrelation function of the second moment $\Phi(t)$, based on the assumption of the three-bond motion, as

$$\Phi(t) = \exp(-t/T_1)\exp(t/T_2)\operatorname{erfc}(t/T_2)^{1/2} \tag{2}$$

where T_1 is the relaxation time of the lattice fluctuation and T_2 the relaxation time of the three-bond motion. The exponential prefactor $\exp(-t/T_1)$ in this equation was added to fit the function to experimental data.[5] In this model, the coupling range of the three-bond motion is considered to be infinitely long. Jones and Stockmayer[17] assumed a finite range of the motional coupling and solved the matrix version of eq 1 (JS model). The autocorrelation function is represented in terms of eigenvectors of the Hückel matrix. Bendler and Yaris[18] again solved the infinite form of eq 1 (equation of plane wave propagation), introducing two cutoff frequencies, which correspond to the size of the motional unit and the motional coupling range (BY model). Skolnick and Yaris[19] developed the BY model by substituting a damping constant of the propagating waves for the longer-range coupling frequency (SY model). Further, to treat chain–chain interactions, they introduced a complex damping constant in this model,[19] and Pant et al.[20] considered the inhomogeneous sites such as side chains or fluorescent probes.

Helfand and his co-workers[21-23] performed the conformational jump analysis by Brownian dynamics simulation and found that the isolated transition and the cooperative counterrotation of the "type 2" transition[24] frequently occur. Hall and Helfand[25] proposed a simplified model that includes two processes of the conformational transitions of a two-state chain (HH model). These two processes consist of an isolated (independent) mode and a cooperative mode and may correspond to the above two processes. The autocorrelation function of this model can be obtained by use of the spin wave as

$$\Phi(t) = \exp(-2\lambda_0 t)\exp(-2\lambda_1 t)I_0(2\lambda_1 t) \tag{3}$$

where λ_0 and λ_1 are the transition rates of the independent and the cooperative modes, respectively, and I_0 is a modified Bessel function of the zeroth order. Viovy et al.[7] improved this model and proposed the generalized diffusion and loss expression (GDL model), in which the first neighbor correlation is taken into account. Note that in both the BY and SY models, the polymer chain is regarded as a continuous wire (the continuous limit is taken), while in the mathematical procedures of the HH (GDL) and JS theories, the discreteness of the diffusion sites remains.

All the models mentioned above include a few phenomenological parameters, and these dynamic parameters are considered to reflect the characters of individual polymer chains. By using these models as tools, we can evaluate the dynamic properties of polymers from experimental data. In this sense, these models are phenomenological or semiempirical. On the other hand, Yamakawa and his co-workers[26] established a nonphenomenological dynamic model as the discrete helical wormlike chain model. In this theory, the physical quantities of dynamics such as the orientation autocorrelation function can be expressed uniquely in terms of several molecular parameters of a helical wormlike chain and its dynamic parameters.

Table I
Various Model Functions Used in This Study

model	$\Phi(t)$
VJGM	$\exp(-t/T_1)\exp(t/T_2)\operatorname{erfc}(t/T_2)^{1/2}$
JS (5-bonds)	$0.578\exp(-t/T_1) + 0.422\exp(-t/T_2)$
BY	$0.5\pi^{1/2}(\operatorname{erfc}(t/T_1)^{1/2} - \operatorname{erfc}(t/T_2)^{1/2})/((t/T_2)^{1/2} - (t/T_1)^{1/2})$
SY	$0.5\pi^{1/2}\exp(-t/T_2)(T_1/t)^{1/2}\operatorname{erf}(t/T_1)^{1/2}$
HH	$\exp(-t/T_1)\exp(-t/T_2)I_0(t/T_2)$
GDL	$\exp(-t/T_1)\exp(-t/T_2)[I_0(t/T_2) + I_1(t/T_2)]$

Table II
Molecular Weights of the Samples

	PMMA-1	PMMA-2	PMMA-3
$M_n \times 10^{-4}$	2.1	12.8	19.0
$M_w \times 10^{-4}$	2.3	15.0	20.7
M_w/M_n	1.11	1.18	1.09

Table I shows the expressions for the orientation autocorrelation function for the models employed in this study. In this table, all the phenomenological parameters are converted to T_1 and T_2, which are both in the dimension of time. As for the JS model, we used $\Phi(t)$ for five-bond coupling to unify the number of variable parameters of all models (two).

III. Experimental Section

Anthracene-labeled PMMA samples used in this study were prepared in the same manner as described previously;[12] anionic polymerization of methyl methacrylate was initiated by (1,1-diphenylhexyl)lithium in THF at −78 °C.[27] After complete exhaustion of the monomer, the living ends were deactivated at −78 °C by a bifunctional terminator 9,10-bis(bromomethyl)anthracene, which had been obtained from 9,10-dimethylanthracene.[28] The polymers were purified by reprecipitation in hexane several times and dried in vacuo. The highest molecular weight sample (PMMA-3 in Table II) was further purified by GPC to eliminate the end-labeled fraction. The molecular weights of these samples were determined by GPC as shown in Table II. The triad tacticity of these polymers was determined by ^{13}C NMR to be 86% syndiotactic. For the measurements of fluorescence emission anisotropy, samples were dissolved in 2-methoxyethanol (methylcellosolve), benzene, and ethyl acetate–tripropionin (glycerol tripropionate) mixed solvents[5] at several mixing ratios. The concentrations of these solutions were kept less than 0.1 wt % to exclude the polymer–polymer interactions as well as the migration of the electronic excited states. All these sample solutions were degassed before measurements were taken.

The apparatus of the nanosecond single-photon counting system used in this study was the same as that reported previously:[12] photomultiplier (PRA Model 1550), time-to-amplitude converter (ORTEC model 457), discriminator (ORTEC model 436, 583), multichannel analyzer (HITACHI model 505), and hydrogen gas filled flash lamp (PRA model 510B) (the pulse width is about 2 ns). To excite the probe, a combination of two filters, UVD-36A and SC-37 (365–390 nm) was used, and a cutoff filter SC-42 was used for detection. A Polaroid HNP'B was used as the polarizing filter. Parallel and perpendicular components of the fluorescence intensity, $I_{\parallel}^{obsd}(t)$, $I_{\perp}^{obsd}(t)$, and the exciting pulse were measured alternately every 60 s to avoid data distortions by the time-drift of the apparatus. This procedure was controlled by a microcomputer (SORD Model M-223). Thus, we could obtain the observed anisotropy ratio $r^{obsd}(t_i)$, as

$$r^{obsd}(t_i) = \frac{I_{\parallel}^{obsd}(t_i) - GI_{\perp}^{obsd}(t_i)}{I_{\parallel}^{obsd}(t_i) + 2GI_{\perp}^{obsd}(t_i)} \tag{4}$$

with

$$t_i = c(i - 1)$$

where c is the channel width (0.152 ns/channel), i the channel number, and G the compensating factor for the anisotropic sensitivity of the photon detector.

Deconvolution procedures were carried out according to the method of Wahl[29] by use of a FACOM M-382 digital computer at the Data Processing Center in Kyoto University. We introduced a channel-shift parameter to eliminate the wavelength effect on the response time of the apparatus. First, we determined the channel-shift parameter and fitted a triexponential function

$$F(t) = a_1 \exp(-t/\tau_1) + a_2 \exp(-t/\tau_2) + a_3 \exp(-t/\tau_3) \quad (5)$$

to the total fluorescence intensity decay $F^{obsd}(t_i) = I_{\parallel}^{obsd}(t_i) + 2I_{\perp}^{obsd}(t_i)$, by the method of nonlinear-least-squares fitting. This time, we used the quasi-Marquardt algorithm in the SALS system.[30] The reduced sum of the squares of the residuals, χ^2, is defined generally as

$$\chi^2 = \frac{1}{n - m}\sum_i w_i[F^{obsd}(t_i) - F^{calcd}(t_i)]^2 \quad (6)$$

where n is the number of data points, m the number of variable parameters, and w_i the weighting factor corresponding to the estimated error. In our case,

$$F^{calcd}(t_i) = \int_0^{t_i} P(T)F(t_i - T)\, dT \quad (7)$$

and

$$w_i = [I_{\parallel}^{obsd}(t_i) + 4G^2 I_{\perp}^{obsd}(t_i)]^{-1} \quad (8)$$

where $P(T)$ is the exciting pulse intensity. The integration in eq 7 was calculated numerically. Thus, we obtained the best-fit parameters of the total intensity. Then, we analyzed the anisotropy decay curves again by using the SALS system. It is well-known that the anisotropy ratio, $r(t)$, is related directly to the orientation autocorrelation function $\Phi(t)$, as

$$r(t) = r_0\Phi(t) \quad (9)$$

where r_0 is the initial anisotropy ratio. So, it follows

$$r^{calcd}(t_i) = \frac{r_0\int_0^{t_i} P(T)\Phi(t_i - T)F(t_i - T)\, dT}{\int_0^{t_i} P(T)F(t_i - T)\, dT} \quad (10)$$

and in this case, w_i is given by[29]

$$w_i = 3F^{obsd}(t_i)/[1 + G + 3Gr^{obsd}(t_i) - 3[r^{obsd}(t_i)]^2 - 2(2G - 1) \times [r^{obsd}(t_i)]^3] \quad (11)$$

Then, χ^2 could be calculated from eq 6, $r^{obsd}(t_i)$ and $r^{calcd}(t_i)$ being substituted for $F^{obsd}(t_i)$ and $F^{calcd}(t_i)$, respectively. In this way, the model functions listed in Table I were tested, and also the phenomenological parameters T_1, T_2 (see Table I), and r_0 were determined.

IV. Results and Discussion

The fluorescence emission decays $[I_{\parallel}(t) + 2I_{\perp}(t)]$ of anthracene introduced in PMMA chains were found to be almost single exponential functions, and fluorescence lifetimes were found to be 9.4 ns in benzene and 10.7 ns in methylcellosolve at 26 °C. Nevertheless, we analyzed them with triexponential functions for the sake of accuracy, as described in the previous section.

The effect of the chain length on polymer local motions is virtually negligible for polymers of sufficiently high molecular weight. Table III shows the average anisotropy ratio for each sample in methylcellosolve. The value of the anisotropy ratio for PMMA-2 ($M_n = 1.28 \times 10^5$) is almost the same as that for PMMA-3 ($M_n = 1.90 \times 10^5$) at every temperature. Therefore, in the molecular weight region of $M_n \geq 1.28 \times 10^5$, the observed motions can be said to be independent of the chain length. With this in mind, we will discuss mainly the results for PMMA-2 below.

Table III
Average Anisotropy Ratio in Methylcellosolve

temp, °C	PMMA-1	PMMA-2	PMMA-3
26	0.136	0.144	0.145
35	0.105	0.125	0.120
45	0.087	0.103	0.102

Table IV
Best-Fit Parameters for PMMA-2 in Methylcellosolve at 26 °C

model	r_0	T_1/ns	T_2/ns	χ^2
VJGM	0.304	29.1	20.1	1.191
JS	0.272	*a*	*a*	1.101
BY	0.268	3.0	175	1.231
SY	0.269	2.9	69.0	1.187
HH	0.266	158	9.0	1.316
GDL	0.271	56.4	4.2	1.143

[a] $\tau_h = 6.38$ ns; $\tau_h = 2/(T_1^{-1} + T_2^{-1})$.

Table IV shows the best-fit parameters for PMMA-2 in methylcellosolve at 26 °C obtained from a time-resolved measurement. The value of r_0 for the VJGM model is higher than those for the other models; this is caused by the steep feature of the initial part of the VJGM decay function (this correlation function really involves an infinitely rapid relaxation process, which seems to be unrealistic). However, aside from the VJGM model, the values of r_0 obtained here are a little higher than those obtained for polystyrene.[7] The reason for this is not clear. We measured the intrinsic viscosity of the methylcellosolve solution, and from the relation of Riseman and Kirkwood,[31] the overall rotational relaxation time was obtained as 374 ns. This is much higher than the obtained value of T_1 for the VJGM model (29.1 ns), thus the relaxation time of the lattice fluctuation, T_1, of the VJGM model is not due to the overall motion. For the JS model, the relaxation time, τ_h, related to the three-bond jump (harmonic mean of T_1 and T_2), is obtained to be 6.4 ns, which is somewhat larger than the relaxation time of the motional unit (T_1) for the BY and SY models. The parameter T_2 of the BY model (this is related to the motional coupling range) is relatively high, being of the same order of the overall motion. We found that this parameter still depends slightly on molecular weight above 1.28×10^5. The parameter T_1 of the SY model is slightly smaller than that of the BY model, and this tendency is always observed for the other data of our experiments. The parameter T_2 of the SY model is the relaxation time related to the damping constant.

For the HH and GDL models, $T_1 > T_2$ is observed; i.e., the cooperative transition occurs more frequently than the isolated transition does. This is contrary to the result of Brownian dynamics simulation.[21] However, we are convinced that our result is realistic from the physical point of view. Indeed, the isolated transition requires large-scale swings of the attached tails. Therefore, such a motion may be strongly inhibited. The exponential factor $\exp(-t/T_1)$ of the correlation functions of the HH and GDL models may rather be interpreted as a contribution of somewhat large-scale motions.

We also fitted the well-known empirical decay function by Williams and Watts,[32] $\Phi(t) = \exp[-(t/\rho)^{\beta}]$, to our data, and found that it agrees with our data fairly well. However, the values of exponent β were dependent on experimental conditions such as temperature or solvent viscosity. Such results may be contrary to the assumption in the recent interpretation of the Williams–Watts function by Bendler and Shlesinger.[33]

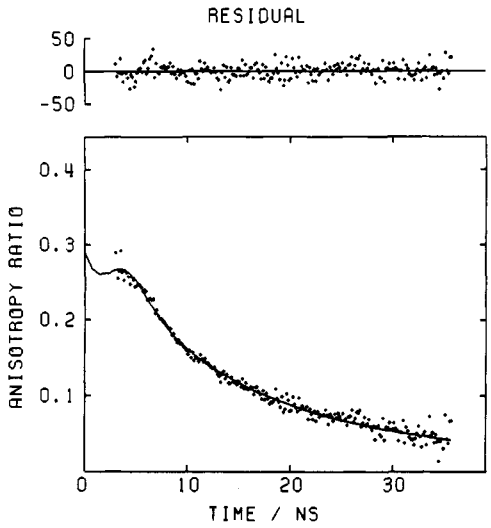

Figure 1. Anisotropy decay for PMMA-2 in methylcellosolve at 26 °C. Dots represent experimental data, and the solid curve indicates the theoretical decay convoluted with the best-fit parameters for the VJGM model shown in Table IV. The weighted residuals are also plotted on an arbitrary scale.

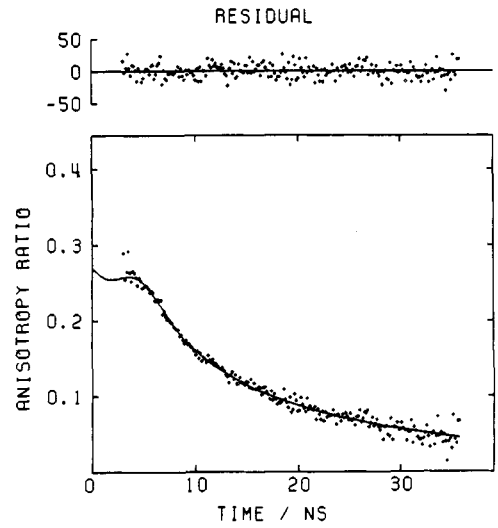

Figure 2. Anisotropy decay for the sample of Figure 1. The solid curve indicates the theoretical decay convoluted with the best-fit parameters for the JS model.

The values of χ^2 (Table IV) show that the agreement is fairly good for the JS and GDL models compared with the BY and SY models, as we reported previously for the low molecular weight sample ($M_n = 2.07 \times 10^4$). Three examples of anisotropy decay fitted with the theoretical functions of the VJGM, JS, and SY models are shown in Figures 1, 2, and 3, respectively. Table IV also shows that χ^2(BY) > χ^2(SY), and χ^2(HH) > χ^2(GDL). Thus both the improvements in the damped orientation model and in the generalized diffusion and loss model seem to be successful (at low viscosities, this is not the case, as will be shown later).

Figure 4 shows a histogram representation of χ^2 for the BY, SY, JS, and GDL models at different temperatures. As we mentioned in section II, we can call the BY and SY models the continuous models and the JS and GDL models the discrete models. Again, as shown in this figure, agreement between theory and experiment is better for discrete models than for continuous models in general. This is consistent with our previous result[12] for the low molecular weight sample, and this tendency is clear at low temperatures.

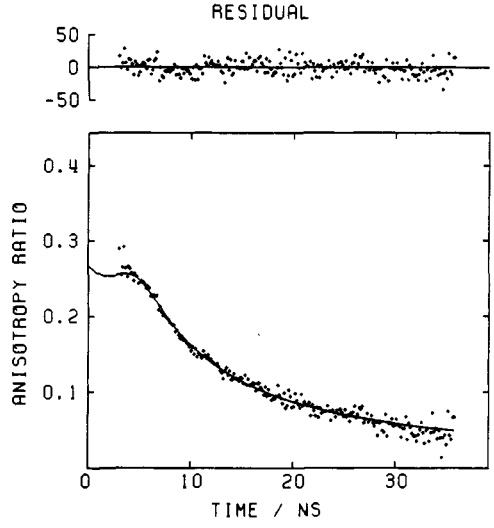

Figure 3. Anisotropy decay for the sample of Figure 1. The solid curve indicates the theoretical decay convoluted with the best-fit parameters for the SY model.

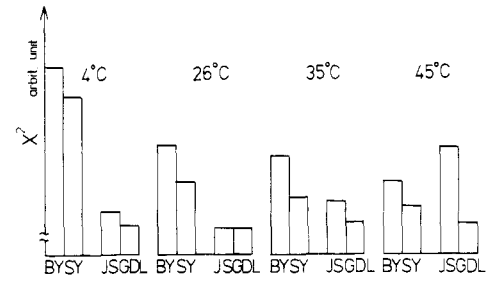

Figure 4. Histogram representation of the values of χ^2 on arbitrary scales for the BY, SY, JS, and GDL models at different temperatures for PMMA-2 in methylcellosolve. The values for the BY and SY models are relatively high compared with those for the JS and GDL models.

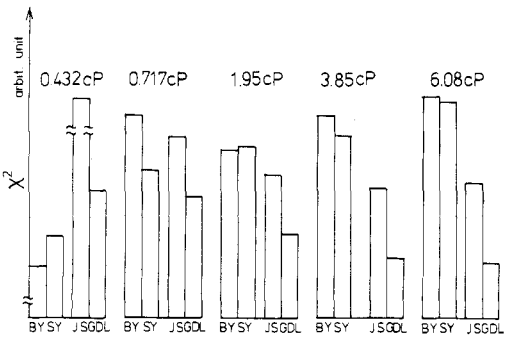

Figure 5. Histogram representation of the values of χ^2 on arbitrary scales at different viscosities for PMMA-2 at 25 °C. Mixtures of ethyl acetate–tripropionin were used as solvents.

Figure 5 shows a histogram representation of χ^2 at various solvent viscosities. These data were obtained in mixed solvents (ethyl acetate–tripropionin) at several mixing ratios at 25 °C. In this case, at high viscosities, the discrete models show good agreement, and at low viscosities, the continuous models work better. Thus we have found that the discrete models are suitable for the observed local motions at low temperatures or at high viscosities.

However, we cannot draw directly from the above fact the conclusion that the distribution of the relaxation times, i.e., of the motional modes of conformational transitions, depends on temperature or solvent viscosity, because the observing time window of the anisotropy decays in the experiments may also vary with temperature or solvent viscosity. Indeed, all our results discussed above were of fixed windows. Thus, we examined the truncation effect

Table V
Values of χ^2 for Various Time Truncations for PMMA-3 in Methylcellosolve at 26 °C

	model			
time window/ns	JS	GDL	BY	SY
A, 3–9.7	1.277	1.251	2.482	2.159
B, 3–24	1.312	1.313	1.417	1.386
C, 10–37	1.008	1.000	0.996	0.998
D, 15–37	1.010	1.001	0.997	1.000

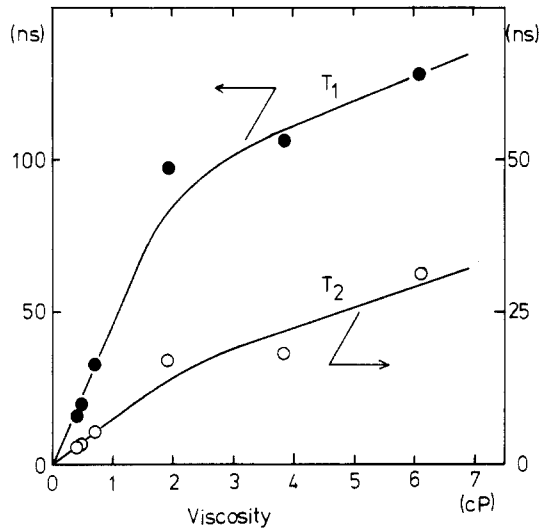

Figure 6. Plots of the dynamic parameters T_1 and T_2 of HH model against the solvent viscosity. The data were obtained at 25° C.

on the behavior of each model (Table V). The data used are for PMMA-3 in methylcellosolve at 26 °C, and the curve fittings were executed with the four models in the truncated time regions shown in the table. As expected, the results indicate that in the short time regions such as A and B, the discrete models show good agreement compared with the continuous models. Thus, it can be said with certainty that at low temperatures or at high viscosities, relatively large-scale motions (they may be called the semiglobal motions) do not relax in the time region of the fluorescence lifetime of anthracene and that one observes, therefore, relatively small-scale motions contributed by the local conformational jumps (they may be called the local motions) in such a case.

In Figure 6, we plot the two parameters of the HH model against solvent viscosity. We obtained these parameters by introducing a base-line parameter a in the HH model function as

$$\Phi(t) = (1 - a) \exp(-t/T_1) \exp(-t/T_2) I_0(t/T_2) + a \quad (12)$$

to eliminate the unrelaxed component which can be regarded as the contribution of the semiglobal motions at high viscosities. This type of equation for a time-correlation function was proposed by Weber and Helfand[34] to fit to their computer simulation results. At low viscosities, the values of the base-line parameter a were obtained to be nearly zero. The profiles of the curves represented in Figure 6 are quite analogous to those obtained by Biddle and Nordström[35] for polystyrene. Apparently, there exist two regions of viscosity. According to Kramers,[36] the motions in the lower viscosity part are in the diffusion limit, and in the higher viscosity part, the activated state plays a role, namely, the motions are in the nondiffusion limit in this case.[37] As is often the case with the diffusion limit, the molecular motions are expected to associate with a large amount of friction. Such motions should therefore

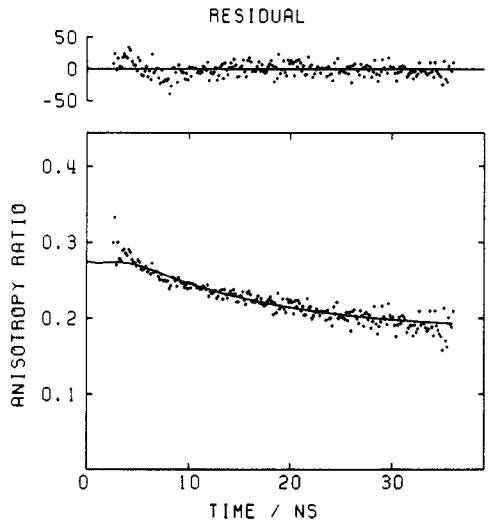

Figure 7. Anisotropy decay for PMMA-2 at a high solvent viscosity (3.85 cP) convoluted with the best-fit parameters for the GDL model. The data were obtained at 25 °C. In the plot of the weighted residuals, a slight deviation is seen in the rapid time region even for this model (see text).

involve large polymer segments. Thus, from our results, in the low viscosity region (<2 cP), the semiglobal motions containing large polymer segments are mainly observed, and the local conformational jump processes occur in such a very rapid time scale that they cannot be detected by our experimental equipment. On the other hand, in the high viscosity region (>2 cP), the local conformational processes, which require only a small amount of friction, relax just in the virtual time window of the anthracene probe. Thus, a highly viscous medium is required to detect such local motions. We now turn to Figure 5. In this figure, the values of χ^2 are relatively small for the discrete models at high viscosities. Therefore, we can conclude that the discrete models, in which the discrete motional modes are taken into account in certain mathematical fashions, are appropriate to treat the local conformational motions. In other words, these discrete models can correctly account for the local motions which belong to the low-friction limit of Kramers. Indeed, in the nanosecond time scale, the discrete chemical structure of polymer chains, or even that of solvent molecules, should be taken into account.

Nevertheless, we feel that the JS and GDL models are not necessarily sufficient for treating the local motions, for a slight systematic deviation is still observed in the early time region even for such discrete models at high viscosities (see Figure 7). This deviation suggests that a real polymer chain possesses some more complicated elementary processes than those assumed in the discrete models and that such processes are intrinsic to each kind of polymer chain. It may also be considered that some rapid processes such as librational motions[38] are detected in the high viscosity region. Anyway, more detailed models based on the chemical structures of real polymer chains are required to scrutinize the local motions.

The activation energies of T_1 and T_2 of the HH model for PMMA-2 in methylcellosolve were found to be 5.3 and 5.5 kcal mol^{-1}, respectively. Thus, the activation energy for the isolated (uncorrelated) transition is almost the same as for the cooperative (correlated) transition. This result corresponds to the conclusion from the excimer emission study[16] as well as from the Brownian dynamics simulations.[21,39] However, in the temperature range of our experiment, the solvent viscosity is less than 2.1 cP, and in this viscosity region, the semiglobal motions are detected as mentioned above. Further experiments are required to

Table VI
Best-Fit Parameters for PSY, BY, and SY Models for PMMA-2 in Ethyl Acetate–Tripropionin at 25 °C

model		viscosity/cP 0.432	0.496	0.717	1.95	3.85	6.08
PSY	T_1/ns	0.88	1.07	1.80	6.60	33.5	30.4
	T_2/ns	15.8	20.8	37.6	788	600	4.2×10^3
	T_3/ns	380	300	303	684	700	6.2×10^3
	χ^2	1.068	0.883	1.382	1.717	1.624	1.067
BY	T_1/ns	0.93	1.12	1.81	5.37	26.6	29.9
	T_2/ns	21.8	27.1	45.5	2.0×10^3	1.0×10^3	3.0×10^3
	χ^2	1.034	0.873	1.430	1.608	1.580	1.056
SY	T_1/ns	0.82	0.99	1.64	5.08	22.8	29.7
	T_2/ns	12.4	15.3	24.7	500	1.0×10^3	850
	χ^2	1.116	0.906	1.289	1.610	1.527	1.053

evaluate the activation energies for real local motions.

We now discuss the model proposed by Pant et al.[20] (referred to as PSY model). They considered the effect of an inhomogeneous site of the fluorescent probe on the plane wave propagation. Their expression for the autocorrelation function is given by

$$\Phi(t) = \exp(-t/T_2)[0.5(\pi T_1/t)^{1/2} \operatorname{erf}(t/T_1)^{1/2} - (\pi/2) \times (T_1/T_3)^{1/2} \exp(t/T_3) \operatorname{erfc}(t/T_3)^{1/2} + T_1/T_3[\exp(-t/T_1) - (\pi t/T_1)^{1/2} \operatorname{erfc}(t/T_1)^{1/2}]]/(1 - (T_1/T_3)^{1/2} \tan^{-1}(T_3/T_1)^{1/2}) \quad (13)$$

where T_1 and T_2 have the same meaning as those in the SY model and T_3 is the relaxation time relating to a damping by the fluorescent probe. In this case, $T_1/T_3 < 1$ is required. Using this expression, we have determined the parameters T_1, T_2, and T_3 by the same method as described in the experimental section, and the results are shown in Table VI. The parameters of the BY and SY models are also given in this table for comparison. At low viscosities (≤0.717 cP), the values of T_1 and T_2 of the PSY model are intermediate between those of the BY and SY models, and the difference between these parameters and those of the BY or SY model may not be significant. The values of χ^2 are also intermediate between those of the BY and SY models. Thus, the improvement of this model is not necessarily successful in spite of the good three-parameter fit. Hence, the probe does not perturb the local motions of the bare polymer chain significantly within the assumption of the PSY theory. At high viscosities (≥1.95 cP), the values of χ^2 of the PSY model are relatively high compared with those of the BY and SY models. This indicates that the PSY model is inadequate for the motions observed at these viscosities. Now, note from Table VI that at low viscosities (0.432 and 0.496 cP), χ^2(SY) > χ^2(BY) is observed. Also we found that χ^2(GDL) > χ^2(HH) at these viscosities. The same feature is reported for polyisoprene in low viscosity solvents (hexane and cyclohexane) by the transient holographic grating experiments.[40] The reason for these results is not clear.

At this stage, we attempt to evaluate the chain stiffness from our data. Chain stiffness is one of the most important properties and it reflects well the "chain character". This time, we employ the HH model for convenience. The cross-correlation function $c(x,t)$ of this model is expressed as[25]

$$c(x,t) = \exp(-t/T_1) \exp(-t/T_2) I_{|x|}(t/T_2) \quad (14)$$

where x is the distance between the two correlating bonds (or segments) along the chain. We define the correlation integral $I(x)$ as

$$I(x) = \int_0^\infty c(x,t)\, dt \quad (15)$$

This integral can be considered as a measure of the correlation strength at a distance x along the chain. From eq 14 and 15 we obtain

$$I(x) = \frac{T_2[(1 + T_2/T_1)^2 - 1]^{-1/4}}{(\sinh s)^{1/2}} e^{-s|x|} \quad (16)$$

where

$$s = \cosh^{-1}(1 + T_2/T_1) \quad (17)$$

It is readily seen that the decay rate of the motional correlation strength against x is $s = \cosh^{-1}(1 + T_2/T_1)$; i.e., s^{-1} represents the extent of motional correlation (coupling range). Hence, the independent transition rate λ_0 [$=(2T_1)^{-1}$] narrows the motional coupling range, and in contrast, the cooperative transition rate λ_1 [$=(2T_2)^{-1}$] extends it. Table VII shows the value of s^{-1} for PMMA-2 in ethyl acetate solvent at 25 °C, which is obtained from T_1 and T_2 of the HH model. For comparison, the values for polystyrene under the same condition calculated from the results of Viovy et al.[7] are also shown in this table. The molecular weight of this polystyrene is 5.7×10^4. The best-fit parameters used in the calculations were T_1 = 15.8 ns, T_2 = 2.76 ns for PMMA and T_1 = 5.99 ns, T_2 = 3.56 ns for polystyrene. These values clearly show that the correlating range of the motions for PMMA extends to a longer distance than that for polystyrene does. The stiffness parameter, λ^{-1}, is considered as the most appropriate one to evaluate static chain stiffness.[41] According to the results of numerical calculations,[42] λ^{-1} = 65.6 Å for PMMA (syndiotactic) and 37.5 Å for polystyrene (syndiotactic) at 300 K, i.e., s-PMMA is stiffer than s-polystyrene. Our result obtained above is qualitatively consistent with this relation since the motional coupling range may be directly influenced by the static stiffness. Thus, we could estimate the static stiffness from the dynamic parameters T_1 and T_2 of the HH model.

Table VII
Values of s^{-1} and $I(0)$ for PMMA and Polystyrene in Ethyl Acetate at 25 °C

	PMMA	polystyrene[a]
s^{-1}	1.716	0.959
$I(0)$/ns	4.48	2.87

[a] Calculated from the parameters obtained by Viovy et al.[7]

Yamakawa et al.[43] suggested the relationship between the static and the dynamic chain stiffness, and recently, such a problem has received considerable interest. In the present case, the dynamic chain stiffness may be evaluated by $I(0)$, which means the correlation time of the polymer segment. Table VII also shows the values of $I(0)$ which are obtained from T_1 and T_2 of the HH model. One can see that the dynamic stiffness parameter $I(0)$ of PMMA is larger than that of polystyrene.

However, the PMMA and the polystyrene compared above have different molecular weights (chain length), so

a possibility may exist that the obtained value of $I(0)$ reflects partially such an effect. We feel that from the practical point of view, the dynamic stiffness parameter, which is independent of molecular weight (chain length), is not easy to evaluate. The dynamic stiffness is considered to be represented by a reciprocal of a sum of all the possible elementary jump rates. These rates are essentially independent of the chain length. It is necessary to elucidate concretely the local elementary processes in the real polymer chains in order to extract such local motions from experimental data. This is a future problem.

V. Conclusion

We have investigated the local motions of PMMA chains of sufficiently high molecular weight in dilute solutions by the fluorescence depolarization method. At low temperatures or at high viscosities of solvent, relatively small-scale motions belonging to the low-friction limit can be observed. It is revealed that these local motions can be well explained by the discrete models, in which the discrete motional modes are taken into account. The stiffness of the polymer chains, which characterizes each kind of polymer chain, can be evaluated by using the dynamic parameters of the HH model, and it is shown that both the static and the dynamic stiffness parameters of PMMA are larger than those of polystyrene.

Acknowledgment. We thank Dr. Q. Tran-Cong for valuable suggestions and valuable discussions. We also thank Dr. M. Sawamoto for characterizing our samples by GPC. This work was supported by a Grant-in-Aid for Scientific Research (No. 62470094) from the Ministry of Education.

References and Notes

(1) Flory, P. J. *Statistical Mechanics of Chain Molecules*; Interscience Publishers: New York, 1969.
(2) Perrin, F. *J. Phys. Radium* **1934**, *5*, 497.
(3) Anufrieva, E. V.; Gotlib, Yu. Ya. *Adv. Polym. Sci.* **1981**, *40*, 1 and papers cited therein.
(4) O'Conner, D. V.; Phillips, D. *Time-Correlated Single-Photon Counting*; Academic: London, 1984.
(5) Valeur, B.; Monnerie, L. *J. Polym. Sci., Polym. Phys. Ed.* **1976**, *14*, 11.
(6) Valeur, B.; Jarry, J. P.; Geny, F.; Monnerie, L. *J. Polym. Sci., Polym. Phys. Ed.* **1975**, *13*, 667. Valeur, B.; Monnerie, L.; Jarry, J. P. *Ibid.* **1975**, *13*, 675.
(7) Viovy, J. L.; Monnerie, L.; Brochon, J. C. *Macromolecules* **1983**, *16*, 1845.
(8) Viovy, J. L.; Monnerie, L. *Polymer* **1986**, *27*, 181.
(9) Viovy, J. L.; Monnerie, L.; Melora, F. *Macromolecules* **1985**, *18*, 1130. Viovy, J. L.; Frank, C. W.; Monnerie, L. *Ibid.* **1985**, *18*, 2606.
(10) Millar, D. P.; Robbins, R. J.; Zewail, A. H. *Proc. Natl. Acad. Sci. U.S.A.* **1980**, *77*, 5593; *J. Chem. Phys.* **1981**, *74*, 4200; **1982**, *76*, 2080.
(11) Barkley, M. D.; Zimm, B. H. *J. Chem. Phys.* **1979**, *70*, 2991.
(12) Sasaki, T.; Yamamoto, M.; Nishijima, Y. *Makromol. Chem., Rapid Commun.* **1986**, *7*, 345.
(13) Kirkwood, J. G. *Recl. Trav. Chim. Phys-Bas* **1949**, *68*, 649; *J. Polym. Sci.* **1954**, *12*, 1.
(14) Schatzki, T. F. *J. Polym. Sci.* **1962**, *57*, 496.
(15) Mashimo, S.; Nakamura, H.; Chiba, A. *J. Chem. Phys.* **1982**, *76*, 6342.
(16) Liao, T.-P.; Morawetz, H. *Macromolecules* **1980**, *13*, 1228.
(17) Jones, A. A.; Stockmayer, W. H. *J. Polym. Sci., Polym. Phys. Ed.* **1977**, *15*, 847.
(18) Bendler, J. T.; Yaris, R. *Macromolecules* **1978**, *11*, 650.
(19) Skolnick, J.; Yaris, R. *Macromolecules* **1983**, *16*, 266; and preceding papers cited therein.
(20) Pant, B. B.; Skolnick, J.; Yaris, R. *Macromolecules* **1985**, *18*, 253.
(21) Helfand, E.; Wasserman, Z. R.; Weber, T. A. *Macromolecules* **1980**, *13*, 526.
(22) Skolnick, J.; Helfand, E. *J. Chem. Phys.* **1980**, *72*, 5489. Helfand, E.; Skolnick, J. *Ibid.* **1982**, *77*, 5714.
(23) Helfand, E.; Wasserman, Z. R.; Weber, T. A.; Skolnick, J.; Runnels, J. H. *J. Chem. Phys.* **1981**, *75*, 4441.
(24) Helfand, E. *J. Chem. Phys.* **1971**, *54*, 4651.
(25) Hall, C. K.; Helfand, E. *J. Chem. Phys.* **1982**, *77*, 3275.
(26) Yamakawa, H.; Yoshizaki, T. *J. Chem. Phys.* **1981**, *75*, 1016; and succeeding papers.
(27) Anderson, B. C.; Andrews, G. D.; Arthur, P., Jr.; Jacobson, H. W.; Melby, L. R.; Playtis, A. J.; Sharkey, W. H. *Macromolecules* **1981**, *14*, 1599.
(28) Berner, E.; Gramstad, T.; Vister, T. *Acta Chem. Scand.* **1953**, *7*, 1255.
(29) Wahl, Ph. *Biophys. Chem.* **1979**, *10*, 91.
(30) Nakagawa, T.; Oyanagi, Y. *Saishou Nijiyou-hou niyoru Jikken-Data Kaiseki*; Tokyo Daigaku Shuppan-kai: Tokyo, 1982.
(31) Riseman, J.; Kirkwood, J. G. *J. Chem. Phys.* **1949**, *17*, 442.
(32) Williams, G.; Watts, D. C. *Trans. Faraday Soc.* **1971**, *66*, 80.
(33) Bendler, J. T.; Shlesinger, M. F. *Macromolecules* **1985**, *18*, 591.
(34) Weber, T. A.; Helfand, E. *J. Phys. Chem.* **1983**, *87*, 2881.
(35) Biddle, D.; Nordström, T. *Arkiv Kemi* **1970**, *32*, 359.
(36) Kramers, H. A. *Physica* **1940**, *7*, 284.
(37) Cerf, R. *Chem. Phys. Lett.* **1973**, *22*, 613.
(38) Zinsli, P. E. *Chem. Phys.* **1977**, *20*, 299.
(39) Perchak, D.; Weiner, J. H. *Macromolecules* **1981**, *14*, 785.
(40) Hyde, P. D.; Waldow, D. A.; Ediger, M. D.; Kitano, T.; Ito, K. *Macromolecules* **1986**, *19*, 2533.
(41) Yamakawa, H. *Macromolecules* **1977**, *10*, 692.
(42) Yamakawa, H.; Shimada, J. *J. Chem. Phys.* **1979**, *70*, 609. Fujii, M.; Nagasaka, K.; Shimada, J.; Yamakawa, H. *Macromolecules* **1983**, *16*, 1613.
(43) Yamakawa, H.; Yoshizaki, T.; Fujii, M. *J. Chem. Phys.* **1986**, *84*, 4693.